PbO–GeO$_2$ rib waveguides for photonic applications

V.D. Del Cacho [a,*], D.M. da Silva [a], L.R.P. Kassab [b], A.L. Siarkowski [a], N.I. Morimoto [a]

[a] *Departamento de Engenharia de Sistemas Eletrônicos, Escola Politécnica, Universidade de São Paulo, São Paulo, SP, Brazil*
[b] *Laboratório de Vidros e Datação, Faculdade de Tecnologia de São Paulo, CEETEPS/UNESP, São Paulo, SP, Brazil*

ARTICLE INFO

ABSTRACT

This work presents for the first time to our knowledge the fabrication and characterization of rib waveguides produced with PbO–GeO$_2$ (PGO) thin films. The target was manufactured using pure oxides (60 PbO–40 GeO$_2$, in wt%) and amorphous thin films were produced with the RF sputtering technique. PGO thin films present small absorption in the visible and in the near infrared and refractive index of ~2.0. The definition of the rib waveguide structure was made using conventional optical lithography followed by plasma etching, performed in a Reactive Ion Etching (RIE) reactor. Light propagation mode in the waveguide structure was analyzed using integrated optic simulation software. Optical loss measurements were performed to determine the propagation loss at 633 nm, for ribs with height of 70 nm and width of 3–5 μm; experimental values around 2 dB/cm were found for the propagation loss and confirmed the theoretical calculations. The results obtained demonstrate that PGO thin films are potential candidates for application in integrated optics.

Published by Elsevier B.V.

1. Introduction

Optical waveguides based in heavy metal oxide glasses are attractive candidates for photonics and integrated optics because of their high linear refractive index that can favor the confinement of the light when used in combination with low refractive index materials [1]. Heavy metal germanate glasses have proved to be promising materials for photonics applications because they combine many interesting properties such as high chemical durability, temperature stability and large transparency window in the infrared region [2,3]. Moreover, germanate glasses have higher refractive index (~2.0) and relatively lower phonon energy (800–900 cm^{-1}) than those of silicate, borate and phosphate glasses [4–6].

In particular the 60 PbO–40 GeO$_2$ (in wt%) composition presented in this work has been extensively studied by the authors. When doped with trivalent rare-earth ions, these germanate glasses exhibit strong photoluminescence being potential candidates for applications in solid state lasers and optical amplifiers [7–9]. Nucleation of metallic nanoparticles was also demonstrated recently in germanate glasses with the same composition and the enhancement of the photoluminescence due to silver and gold nanoparticles was reported for samples doped with Pr^{3+}, Er^{3+}, Eu^{3+}, Er^{3+}/Yb^{3+} and Yb^{3+}/Tm^{3+} [10–14]. The nucleation of silver and gold nanoparticles in germanate thin films produced with the sputtering technique by means of a 60 PbO–40 GeO$_2$ (in wt%) vitreous

target was reported [15] as well as the growth of the near-infrared nonlinearity in the presence of Cu nanoparticles [16]. So these considerations led to the choice of the 60 PbO–40 GeO$_2$ (in wt%) composition for the rib waveguides studied in this work.

Rib waveguides have become of great importance in integrated optics due to their capability of laterally confining the optical field. These characteristics make them extremely convenient as building blocks for devices such as sensors, lasers, amplifiers, directional couplers and others [17,18]. However, the production of high quality optical waveguides is not straightforward and, in particular, surface roughness constitutes a major concern [19,20].

In this work, the production and characterization of PbO–GeO$_2$ (PGO) rib-type waveguides are investigated for the first time, using thin films produced by RF sputtering deposition and characterized by a variety of techniques. In particular, scanning electron microscopy (SEM) was essential to optimize the processes involved in the production the waveguides by means of the investigation of the geometry and sidewall of the waveguides. The thin film waveguides were produced on a silicon substrate using conventional microelectronic procedures: chemical cleaning, thermal oxidation, sputtering deposition, optical lithography and plasma etching.

The thickness and the refractive index were measured by profilometry and ellipsometry, and the roughness of the films surface was determined by atomic force microscopy (AFM). The transmission spectra of the films were obtained with a spectrophotometer.

2. Experimental procedure

Rib waveguides were fabricated by RF sputtering deposition, lithography and plasma etching processes of the PGO core. The width of core waveguides was in the range of 1–10 μm.

* Corresponding author.
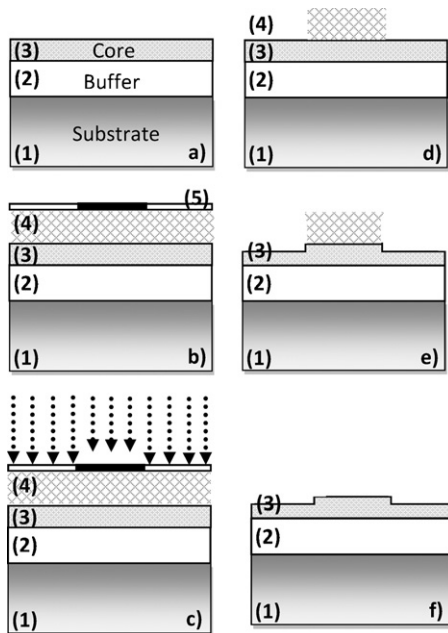*E-mail address:* vainessacacho@gmail.com (V.D. Del Cacho).

Fig. 1. The process steps used for the fabrication of the rib waveguide in PGO thin film. (1) The silicon wafer, (2) the SiO$_2$ buffer-layer used to isolate the PGO core from the substrate, (3) the PGO sputtered film or core, (4) the photoresist, (5) the lithographic mask. (a) The starting stacked structure, as grown on top of Si wafer; (b) the structure after resist spinning and masking; (c) the exposed photoresist; (d) after resist development; (e) after RIE of the PGO layer; (f) the final rib waveguide structure after photoresist removal.

2.1. Waveguides structure

The fabrication process steps are sketched in Fig. 1. The processes steps are scheduled as follows: (a) the starting stacked structure, as grown on top of Si wafer; (b) the structure after resist spinning and mask alignment; (c) the exposed photoresist; (d) after resist development; (e) after Reactive Ion Etching (RIE) of the PGO layer; (f) the final rib waveguide structure after photoresist removal.

Lateral mode confinement is provided by ribs with height and width etched atop the core film. Thus light propagation in the rib region experiences a slightly larger effective index than that on the left and right sides of the rib, preventing the lateral spreading that normally occurs in planar waveguides [17,18,21]. The description of the fabricated rib waveguides dimensions are listed in Table 1.

2.2. Film deposition

The target was manufactured using pure oxides: 40 GeO$_2$–60 PbO (in wt%). The oxide powders were mixed and then submitted to ~400 kgf/cm^2 uniaxial press, followed by sinterization at 750 °C for 10 h. Silicon wafers with 76.2 mm diameter with resistivity between 1 and 10 Ω cm, p type, (1 0 0) orientation were used as substrates. The fabrication sequence starts with a thermal oxidation (at 1150 °C) process of 1 μm thick silicon oxide buffer layer in the silicon wafers.

The core thin films were produced using the RF magnetron sputtering technique at room temperature using a PbO–GeO$_2$ target (diameter 2″, thickness 4 mm). The sputtering was carried out with an Argon gas (flow 18 sccm), at 5 mTorr pressure and RF power of 50 W. The deposition time was 3 h and the distance between target and substrate was 14 cm.

The PGO films deposited were annealed in a furnace at 420 °C for 3 h, because the most sputter-deposited films require long post-annealing steps to produce defect-free stoichiometric films [22]. The annealing procedure is also important to compensate for O$_2$ loss during the sputtering process and enhance the transparency of the thin films.

Table 1
Description of the rib waveguide dimensions produced.

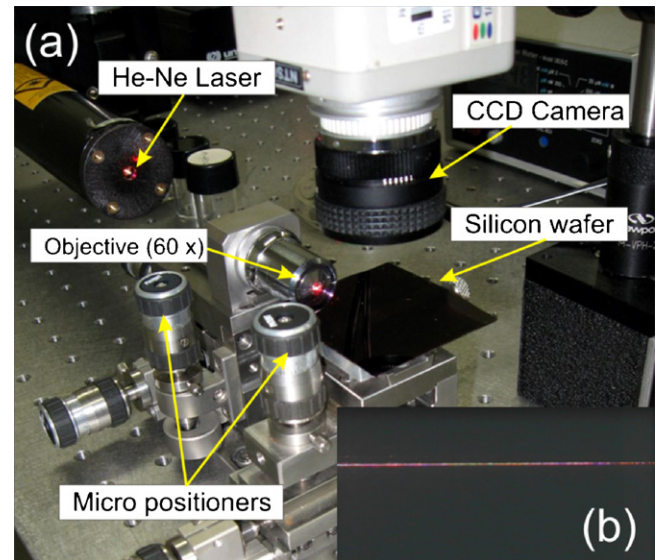| Materials	Function	Dimensions (μm)
SiO$_2$	Isolation layer	1
PbO–GeO$_2$	Core layer	0.296
PbO–GeO$_2$	Rib width	3, 5 and 10
PbO–GeO$_2$	Rib height	0.073
Si	Substrate	380

Fig. 2. Image of the experimental setup (a) and the guided light in a GeO$_2$–PbO rib waveguide (b). Optical loss measurements were carried out by coupling the light from a diode laser (633 nm wavelength) into the GeO$_2$–PbO core.

2.3. Optical lithography

The definition of PbO–GeO$_2$ optical waveguides was performed by conventional optical lithography. Using a spinner, the core film was covered by a positive photoresist (V90), which is sensible to ultraviolet light. After deposition the photoresist is pre-baked (at 105 °C for 90 s), in order to evaporate the solvent. A mask containing the lines pattern is aligned with the wafer for UV exposure. The photoresist regions which were exposed to the UV light are removed by a developer solution (MIF 300).

2.4. Plasma etching

The PGO rib-waveguide was defined by SF$_6$ plasma etching that was performed in a Reactive Ion Etching (RIE) reactor with a photoresist mask. The etching parameters were optimized as follows: pressure = 100 mTorr, SF$_6$ flow rate = 25 sccm, RF power = 50 W, etching time = 5 min and DC bias voltage = 25–30 V.

To remove the photoresist the structure was submitted to oxygen plasma with total pressure of 100 mTorr, O$_2$ flow rate of 50 sccm, RF power of 100 W and DC bias voltage of 500 V for 5 min processing time.

The surface morphology of the etched PGO thin film was investigated by scanning electron microscopy (SEM).

2.5. Optical characterization

Optical loss measurements were performed and enabled the determination of the propagation loss at 633 nm (He–Ne Laser). The optical losses during the propagation of the light at 633 nm were measured with an optical mount using a CCD (charge coupled device) camera positioned above the silicon wafer to analyze the light scattering of the rib-waveguide (experimental). Fig. 2 shows the optical setup used for waveguide characterization.

The mode propagation in a GeO$_2$–PbO rib waveguide was analyzed with an integrated optics simulation software [23] to determine the appropriate thickness of the SiO$_2$ buffer and the GeO$_2$–PbO waveguide core layers. The software was also used to determine the depth of the etching necessary to promote the rib over the GeO$_2$–PbO waveguide core for multimode propagation at 633 nm.

3. Results

The final thickness and the refractive index of PGO thin film were measured by profilometry and by ellipsometry and the roughness of the films surface were measured by AFM (atomic force microscopy). The obtained results were used in the simulations to calculate the theoretical propagation losses and are listed in Table 2.

The etched areas roughness of the PGO film increased to 1.9 ± 0.7 nm after the plasma etching process. The rib walls' roughness estimated by SEM images is in the range 30–50 nm [24], while the rib height measured by profilometry is 73 nm.
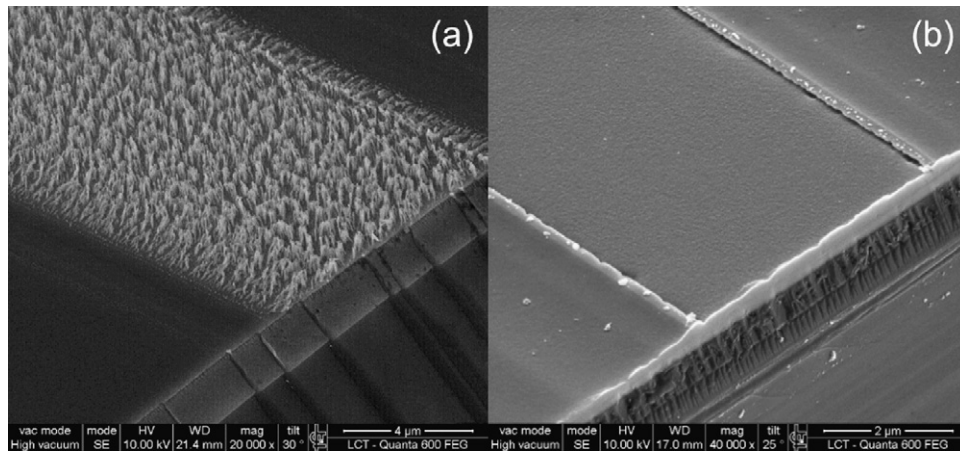
Fig. 3. SEM image of the GeO_2–PbO rib-waveguide: (a) after O_2 plasma (with photoresist waste) and (b) after the use of the microstrip solution.

Table 2
Results obtained by profilometry, ellipsometry ($\lambda = 633$ nm) and AFM.

Material/process	Thickness (nm)	Refractive index	Roughness
GeO_2–PO/sputtering	296 ± 9	1.99 ± 0.02	1.2 ± 0.2
SiO_2/oxidation	1145 ± 5	1.463 ± 0.002	0.7 ± 0.2

Fig. 3 shows SEM sidewall and surface images of the PGO core. The oxygen plasma etching did not remove the photoresist completely and, after that, it was necessary to use the microstrip solution for 15 min.

Fig. 4 shows the optical transmission spectra of PGO films deposited on glass substrates as a function of wavelength.

The spectrum of the PGO film after annealing at 420 °C during 10 h shows high transmittance > 90% (maxima) in the visible region. The features are due to the interference between the light beams reflected on the film and substrate surfaces.

The rib waveguides presented high confinement field and multimode propagation for TE polarized light at 633 nm. The obtained propagation losses (experimental and theoretical values) are listed in Table 3. The experimental results were obtained using the setup presented in Fig. 2 and the theoretical propagation losses were calculated according to Deri et al. [24] using the results presented in Table 2.
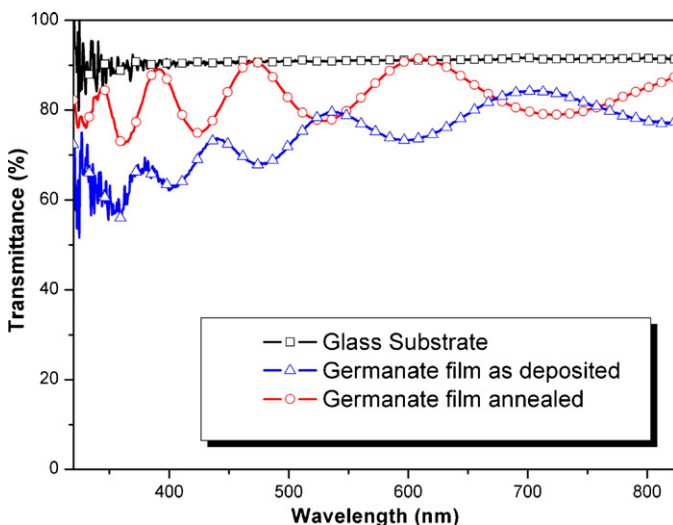
4. Discussion

The results presented demonstrated that the germanate film deposited without annealing showed lower transmittance in the visible range. In this case the film was prepared without oxygen in the chamber, favoring the production of a high number of vacancies in O–Ge–O bonds [25]. Thus, after annealing, the films showed high transparency making them suitable for production of very good quality waveguides.

We performed simulations of optical guiding in the rib structures in order to estimate the propagation losses and compare the results with the experimental ones.

The main source of optical attenuation in such waveguides is the light scattering due to the roughness on the films' interfaces [24]. The propagation losses values depend heavily on the surface and lateral roughness, on the thickness uniformity of the films and on the difference between the refractive index of the different materials present. The experimental value of the propagation loss is in agreement with the calculated one as shown in Table 3. We remark that the simulations did not consider the absorption factor in the waveguide but only the loss by scattering.

The optical simulations showed that for single mode propagation at 633 nm the height of the rib would be of 5 nm. In fact the literature reported waveguides with rib height of this dimension [26] for single mode propagation. Considering the etching rate of the PGO film it would be very difficult to perform the etching and to construct the PGO rib waveguide for single propagation using the procedures presented in this work.

The propagation losses obtained for the PGO rib waveguides (2.2 dB/cm for rib height of 0.07 μm and width of 3–5 μm) are comparable to other waveguides reported in the literature. For example, the propagation loss for a Si_3N_4 rib waveguide with different dimensions, rib height of 0.002 μm and width of 3–5 μm, is 2.2 dB/cm for 633 nm [27] for single mode operation. Another example that should be considered is the propagation loss of a Na_2O–MgO–Al_2O_3–GeO_2 rib waveguide with height of 0.2 μm and width of 12 μm for multimode operation: 0.48 dB/cm for 1482 nm

Fig. 4. GeO_2–PbO film transmission spectra in the UV–Vis region.

Table 3
Results of the propagation loss of the GeO_2–PbO waveguide ($\lambda = 633$ nm and TE polarization).

Rib width (μm)	Measured propagation loss (dB/cm)	Calculated propagation loss (dB/cm)
3–5	2.2	2.18
10	0.6	0.05

[28]. In this case the difference may be attributed to the fact that propagation losses for 633 nm are normally much higher than in the infrared region due to Rayleigh scattering [29]. As far as we are concerned there are no reports in the literature related to germanate rib waveguides for propagation at 633 nm. Only results of germanate planar waveguides were reported for propagation at 633 nm [30–32] and are not used for comparison in this work.

5. Conclusions

This work investigated for the first time, as far as the authors are aware of, rib waveguides based on PbO–GeO$_2$ thin films. The RF sputtering deposition technique was utilized to obtain thin films from glass targets; plasma etching and lithography processes were employed for the production of rib waveguides. Propagation losses of 0.6 dB/cm for 10 μm rib width and of 2.2 dB/cm for 3–5 μm rib widths are in good agreement with the theoretical values obtained in the numerical simulations, and suggest this structure as good candidate for photonic devices applications.

As future works, the authors are considering PGO thin films in combination with metallic nanoparticle for surface plasmon resonant sensors, as well as nanostructured photonic devices.

Acknowledgments

References

[1] D. Munoz-Martin, J. Gonzalo, J.M. Fernandez-Navarro, J. Siegel, C.N. Afonso, Appl. Surf. Sci. 254 (2007) 1111–1114.
[2] S.J.L. Ribeiro, J. Dexpert-Ghys, B. Piriou, V. Mastelaro, J. Non-Cryst. Solids 159 (1993) 213.
[3] J. Wang, J.R. Lincoln, W.S. Brocklesby, R.S. Deol, C.J. Mackechnie, A. Pearson, A.C. Tropper, D.C. Hanna, D.N. Payne, J. Appl. Phys. 73 (1993) 8066.
[4] W.H. Dumbaugh, J.C. Lapp, J. Am. Ceram. Soc. 75 (1992) 2315.
[5] E.M. Vogel, M.J. Weber, D.M. Krol, Phys. Chem. Glasses 32 (1991) 231.
[6] A. Margaryan, M.A. Piliavin, Germanate Glasses: Structure, Spectroscopy and Properties, Artech House, Boston, London, 1993.
[7] L.R.P. Kassab, M.E. Fukumoto, L. Gomes, J. Opt. Soc. Am. B 22 (2005) 1255.
[8] L.R.P. Kassab, W.G. Hora, W. Lozano, M.A.S. de Oliveira, G.S. Maciel, Opt. Commun. 269 (2007) 356.
[9] L.R.P. Kassab, A. de, O. Preto, G. Maciel, W. Lozano, J. Non-Cryst. Solids 351 (2005) 3468.
[10] L.P. Naranjo, C.B. de Araújo, O.L. Malta, P.A.S. Cruz, L.R.P. Kassab, Appl. Phys. Lett. 87 (2005) 241914.
[11] D.M. da Silva, L.R.P. Kassab, S.R. Lüthi, C.B. de Araújo, A.S.L. Gomes, M.J.V. Bell, Appl. Phys. Lett. 90 (2007) 081913.
[12] L.R.P. Kassab, F.A. Bomfim, J.R. Martinelli, N.U. Wetter, J.J. Neto, C.B. de Araújo, Appl. Phys. B 94 (2009) 239.
[13] T.A.A. Assumpção, D.M. da Silva, L.R.P. Kassab, C.B. de Araújo, J. Appl. Phys. 106 (2009) 063522.
[14] L.R.P. Kassab, D.S. da Silva, R. de Almeida, C.B. de Araújo, Appl. Phys. Lett. 94 (2009) 101912.
[15] D.S. da Silva, L.R.P. Kassab, J.R. Martinelli, C.B. de Araújo, J. Non-Cryst. Solids 356 (2010) 2602.
[16] L.A. Gómez, F.E.P. dos Santos, A.S.L. Gomes, C.B. de Araújo, L.R.P. Kassab, W.G. Hora, Appl. Phys. Lett. 92 (2008) 141916.
[17] M. Ohkawa, M. Izutsu, T. Sueta, Appl. Opt. 28 (1989) 5153.
[18] C. Wagner, J. Frankenberger, P.P. Deimel, IEEE Photon. Technol. Lett. 5 (1993) 1257.
[19] S. Mailis, C. Riziotis, J. Wang, E. Taylor, A.A. Anderson, S.J. Barrington, H.N. Rutt, R.W. Eason, N.A. Vainos, C. Grivas, Opt. Mater. 12 (1999) 27.
[20] S.J. Barrington, T. Bhutta, D.P. Shepherd, R.W. Eason, Opt. Commun. 185 (2000) 145.
[21] H. Nishihara, M. Haruna, T. Suahara, Optical Integrated Circuits, McGraw-Hill, New York, 1989.
[22] S. Witanachchi, P.J. Wolf, J. Appl. Phys. 76 (1994) 2185.
[23] BBV – Registered Simulation Programs by BBV Software, Enschede, 1998.
[24] R.J. Deri, E. Kapon, L.M. Schiavone, Appl. Phys. Lett. 51 (1987) 789–791.
[25] V.P. Tolstoy, I.V. Chernyshova, V.A. Skryshevsky, Handbook of Infrared Spectroscopy of Ultrathin Films, John Wiley & Sons, Inc., Hoboken, New Jersey, 2003.
[26] P. Karasiński, C. Tyszkiewicz, Roman Rogoziński, Photon. Lett. Pol. 2 (2010) 40–42.
[27] A.L. Siarkowski, B.V. Borges, N.I. Morimoto, The Electrochemical Society Proceedings, Electronics and Photonics, vol. 2005, The Electrochemical Society Inc., Pennington, NJ, USA, 2005, pp. 380–388.
[28] D.L. Yang, E.Y.B. Pun, H. Lin, Appl. Phys. Lett. 95 (2009) 151106.
[29] G.G. Devyatykh, E.M. Dianov, N.S. Karpychev, S.M. Mazavin, et al., Sov. J. Quantum Electron. 10 (1980) 900.
[30] Z. Yi Yin, B.K. Garside, Appl. Opt. 21 (1982) 4324–4328.
[31] S. Sebastiani, G.N. Conti, S. Pelli, G.C. Righini, Opt. Express 13 (2005).
[32] S. Mailis, C. Riziotis, et al., Opt. Mater. 12 (1999) 27–33.